0.0001), perimeter (151.1 ± 4.3 vs. 179.2 ± 4.1 μm, $P <$ 0.0001), Feret diameter (57.5 ± 1.7 vs. 67.2 ± 1.8 μm, $P <$ 0.001), and minimum Feret diameter (36.4 ± 1.1 vs. 44.1 ± 1.2 μm, $P < 0.0001$) were lower in the 85As2 group than in the control group. A corresponding increase in the expression of muscle-specific E3 ubiquitin ligases (atrogin-1 and MuRF-1; Fig. 3, D–E) and reduction in grip strength were also observed (Fig. 5K). Three Foxo family members present in skeletal muscle (Foxo1, Foxo3, and Foxo4) (49) were upregulated in the gastrocnemius muscles of the 85As2-induced cachectic rats, and the increase in Foxo1 was particularly prominent (Fig. 5, G–I). IGF-1 was upregulated in cachectic rats (nonsignificant) (Fig. 5J). Plasma albumin level decreased in 85As2 (1 × 10^7 cells)-bearing cachectic rats, whereas the level of α1-acid glycoprotein, the murine counterpart of human C-reactive protein, was increased (Fig. 4, A and B). Importantly, tumor removal restored body weight loss, food and water intake, body composition (FFM, FM, and TBW), and grip strength (Fig. 5, A–F and K). Furthermore, tumor removal reduced the increased expression levels of not only atrogin-1 (85As2, 321.2% ± 123.2%; tumor removal, 155.2% ± 40.8%) and MuRF-1 (85As2, 261.5% ± 71.3%; tumor removal, 150.7% ± 27.0%) but also Foxo-1 (85As2, 683.7% ± 368.7%; tumor removal, 140.5% ± 29.6%) in the gastrocnemius muscle (Fig. 5, G–I).

Cytokine levels. To investigate the underlying causes of cancer cachexia, the plasma concentrations of several proinflammatory cytokines were measured. Human LIF levels were remarkably elevated in a cell concentration- and time-dependent manner in rats implanted with 85As2 cells, whereas the levels of human IL-1β, IL-6, and TNFα were not elevated in this model at 12 wk (Table 2). Similar results were obtained in MKN45cl85-implanted rats at 12 wk. Additionally, rat IL-1β, IL-6, KC, and TNFα levels were below detection limits, and IFNγ levels were unchanged in both rat models (data not shown). Moreover, human LIF production was observed in cell culture supernatants from both cell lines, although 85As2 cells produced substantially higher amounts of LIF than MKN45cl85 cells (Table 2). Human IL-8 production was also observed in both cell lines. Furthermore, tumor removal reversed the increase in plasma LIF levels in 85As2-bearing cachectic rats (Fig. 5L).

Gene expression of hypothalamic orexigenic/anorexigenic peptides in the 85As2-induced cachexia model. Cachexia symptoms such as body weight loss and anorexia were induced in rats implanted with 85As2 cells (1 × 10^7 cells; Fig. 6, B and C). Hypothalamic feeding-regulating peptide levels were evaluated 4 wk after implantation of 85As2 cells. Orexigenic peptide

mRNA levels (NPY and AgRP in the ARC, ORX and MCH in the LHA) were higher in 85As2 cachectic rats than in control rats, whereas anorexigenic peptide mRNA levels (POMC and CART in the ARC, CRH in the PVN) were lower in cachectic rats than in control rats (Fig. 6A).

Respiratory metabolism in the 85As2-induced cachexia model. Cachexia symptoms such as body weight loss and anorexia were induced in rats implanted with 85As2 cells (1 × 10^7 cells; Fig. 7, G and H). V̇O_2 was higher in 85As2-induced cachectic rats than in control rats 4 wk after implantation (Fig. 7A). Locomotor activity was noticeably lower during the "active" overnight period in cachectic rats than in control rats (Fig. 7, B and D). RQ, V̇O_2, and metabolic calorie levels were significantly higher in cachectic rats than in control rats during the daytime period, although locomotor activity was not different between the groups during this time period (Fig. 7, C–F).

Rikkunshito ameliorates cachexia in the 85As2-induced cachexia model. Rikkunshito increased food and water intake rates (Fig. 8, A–F) and alleviated body weight loss, FFM, TBW, and total musculature weight loss in 85As2-induced cachectic rats (Fig. 8, G–J).

DISCUSSION

Herein, we established novel stomach cancer cachexia models by implanting nude rats with MKN45cl85 and 85As2 cells, both of which were derived from the human stomach cancer cell line MKN-45. These models enabled us to sequentially evaluate anorexia and body composition changes (low FFM) that correspond to poor QOL in human cancer patients. In addition to anorexia and low FFM, the cachexia models showed significant weight loss, reduced musculature and muscle strength, and abnormal biochemistry (increased inflammatory marker levels and low serum albumin levels), thereby fulfilling the cachexia diagnostic criteria (20). Interestingly, cancer cachexia developed earlier and was more severe in the 85As2-bearing model than in the MKN45cl85-bearing model, indicating that 85As2 cells derived from peritoneal dissemination possessed an enhanced ability to cause cachexia. Indeed, the presence of peritoneal metastasis promotes cachexia and is associated with a poor prognosis and low QOL in patients with advanced-stage stomach cancer. Our 85As2-bearing model may provide a useful tool for further study into the mechanisms and potential treatment of cancer cachexia.

Characterization of the 85As2-induced cachexia rat model showed marked weight loss and reductions in food and water

Fig. 8. Effects of rikkunshito on anorexia and body composition changes in the 85As2-induced cancer cachexia model. Changes in food intake (A), water intake (B), cumulative food intake (C), and cumulative water intake (D) over time. Comparison of food intake (E), water intake (F), body weight (G), FFM (H), TBW (I), and total muscle and fat weight (J) before and after rikkunshito administration. Rats were implanted sc with 85As2 cells in both flanks (1 × 10^7 cells/each site) on day −14. Rikkunshito (1 g·kg^{-1}·day^{-1}) or distilled water was administered orally twice a day for 7 days from day 0. Rats inoculated with saline served as a control group and were similarly administered distilled water. Each data point or bar represents the mean ± SE of 10–11 rats. Differences between saline-implanted and 85As2-implanted rats were evaluated using Student's *t*-test; *$P < 0.05$, **$P < 0.01$, and ***$P < 0.001$ vs. the corresponding control + distilled water-treated group (A, B, and G–J). Differences between rikkunshito and distilled water treatments were evaluated using Student's *t*-test; #$P < 0.05$ and ##$P < 0.01$ vs. the corresponding 85As2 + distilled water-treated group (A, B, and H–J). Differences between groups in the time course of cumulative food and water intake were evaluated using 2-way repeated-measures ANOVA, followed by post hoc Bonferroni test; **$P < 0.01$ and ***$P < 0.001$ vs. the corresponding control + distilled water-treated group; #$P < 0.05$, ##$P < 0.01$, and ###$P < 0.001$ vs. the corresponding 85As2 + distilled water-treated group (C and D). Differences between groups were evaluated using a 1-way ANOVA, followed by post hoc Dunnett's multiple comparison test; **$P < 0.01$ and ***$P < 0.001$ vs. the 85As2 + distilled water-treated group (E and F). Differences before and after administration of either rikkunshito or distilled water were evaluated using the paired *t*-test; #$P < 0.05$, ##$P < 0.01$, ###$P < 0.001$ vs. the corresponding before-administration group (E and G).

intake. Furthermore, 85As2-induced cachexia decreased FFM, FM, and TBW, which was confirmed by histological observations. In the present experimental models, tumor growth or cachexia developed very early. However, young rats (aged 8 wk at the time of implantation) were used; therefore, senescence, which is common in human cancer, may have been a limitation of the study. Although 85As2 cell implantation can cause peritoneal dissemination accompanied by ascites (63), the decreased food intake in our model was not associated with either condition. Reduced FFM in cachectic rats was thought to be caused primarily by wasting skeletal muscle and organ tissues, as evidenced by the reduction in all measured musculature weights, muscle atrophy (e.g., gastrocnemius muscle), and reduced spleen and liver weights. Because intracellular skeletal muscle proteins are degraded primarily by the ubiquitin-proteasome system (2, 16), increased expression of the E3 ubiquitin ligases atrogin-1 and *MuRF-1* likely contributed to skeletal muscle loss by accelerating muscle protein breakdown during cancer cachexia development, as these enzymes have been associated with muscle wasting in other cancer cachexia animal models (2, 16). Moreover, increased expression of atrogin-1 and *MuRF-1* in the gastrocnemius muscles of cachectic rats has been associated with increased expression of *Foxo*, the master regulators of muscle-specific E3 ligases, and increased *Foxo* expression has been shown in cancer cachexia models (49). In our study, *Foxo1*, *Foxo3*, and *Foxo-4* were upregulated in 85As2-induced cachectic rats, and their increased expression was thought to be associated with the increased expression of atrogin-1 and *MuRF-1*. Notably, the elevation of Foxo1 levels was prominent, and its blockade suppressed cachectic muscle atrophy (36). Expression of the protein synthetic factor IGF-I has been reported to decrease in cancer cachexia models (16). However, *IGF-1* expression did not decrease in cachectic rats; rather, it unexpectedly increased, although the increase was not significant. Taken together, our findings indicated that protein degradation pathways in skeletal muscle were activated in 85As2-induced cachectic rats. Importantly, tumor removal reversed the cachexia symptoms, including body weight loss, decreased food and water intake, body composition changes, and increased expression of genes that accelerate muscle protein breakdown such as atrogin-1, *MuRF-1*, and *Foxo-1* in 85As2-bearing cachectic rats. These findings strongly indicated that the 85As2 cancer cell xenograft induced cachexia symptoms.

Increasing evidence suggests that proinflammatory cytokines, including TNFα, IL-1, IL-6, IL-10, and TGFβ, may be involved in the development of cancer cachexia (13, 19, 58). For example, high IL-6 levels have been associated with increased inflammation (20) and weight loss in patients with non-small-cell lung, pancreatic, and prostate cancers (19, 46, 51). However, other studies have suggested that cancer cachexia is not fully attributable to IL-6 levels (53). In the present study, human and rat IL-6 were not detected in the plasma of MKN45cl85- or 85As2-tumor-bearing cachectic rats or in cell culture supernatants, making it unlikely that IL-6 was a causative factor for cancer cachexia in our experimental model. Moreover, human and rat IL-1β and TNFα were not detected in the plasma of tumor-bearing cachectic rats, and human IL-10 and TGFβ were not detected in the cell culture supernatants, which was similar to our previous results in a stomach cancer cachexia mouse model (63). In contrast, plasma levels

of human LIF, a pleiotropic cytokine belonging to the IL-6 family, were markedly elevated in a cell concentration- and time-dependent manner in rats implanted with 85As2 cells. These findings are in agreement with a previous study showing higher LIF levels in a melanoma SEKI-induced cancer cachexia mouse model (39, 40). Furthermore, we found that tumor removal not only abolished the cachexia symptoms induced by 85As2 cells but also decreased plasma LIF levels to below detectable levels. Therefore, our findings strongly suggested that LIF is a cachectic factor in the 85As2-bearing cachexia model. To date, genetic polymorphisms of cytokines such as IL-1β, IL-8, and IL-10 have been implicated in cachexia pathogenesis in stomach cancer patients (5, 26, 54). Our study is the first to associate LIF with stomach cancer cachexia. Although clinical evaluation of LIF is currently ongoing, LIF may be a biomarker of pathogenesis and a therapeutic target for peritoneal dissemination and cachexia in stomach cancer.

LIF and its receptor LIF-R, a heterodimeric receptor complex consisting of the ligand-specific LIF-R and signal-transducing gp130 subunit (3), are expressed in POMC neurons in the ARC and have been shown to impact signaling in the hypothalamus. LIF has been shown to inhibit food intake by directly activating POMC neurons in the ARC and stimulating the release of α-melanocyte-stimulating hormone, which in turn transduces anorexigenic signals (27). Importantly, the blood-brain barrier is relatively permissive in the ARC, allowing the neurons to access circulating macromolecules. In fact, Pan et al. (47) showed that peripherally administered LIF reached the brain and spinal cord by crossing the blood-brain barrier. Taken together, these findings suggested that LIF produced by 85As2 and MKN45cl85 cell implantation induced cachexia symptoms, including anorexia, in the present study by affecting LIF receptor signaling pathways in POMC neurons in the ARC. Moreover, LIF may contribute to differences in the onset and severity of cachexia in the 85As2 and MKN45cl185 cachexia models. However, further study is necessary to determine the contribution of other cachectic factors to the varying degrees of cancer cachexia in these models.

In the present study, hypothalamic levels of orexigenic peptide mRNAs (*NPY* and *AgRP* in the ARC, *ORX* and *MCH* in the LHA) were increased in the 85As2-induced cachexia model, whereas the levels of anorexigenic peptide mRNAs (*POMC* and *CART* in the ARC, *CRH* in the PVN) were decreased. Previous studies have shown that hypothalamic NPY release is reduced and that the feeding response to hypothalamic injection of NPY is attenuated in anorectic tumor-bearing rats despite increased hypothalamic *NPY* mRNA expression (9–12, 38). Moreover, proinflammatory signals (e.g., IL-1β) have been shown to decrease AgRP secretion but increase *AgRP* gene transcription (50). Thus, despite increases in hypothalamic *NPY* and *AgRP* mRNA expression, the anorexia induced in our model may involve impairment of NPY and AgRP release or feeding response to NPY. Interestingly, our previous study using a cisplatin-induced cachexia rat model yielded contrasting results to those of the 85As2 model, although both models exhibited decreased food intake. In the cisplatin-induced cachexia model, hypothalamic orexigenic peptide mRNA levels decreased and anorexigenic peptide mRNA levels increased (65). Cisplatin has been shown to reduce the secretion of ghrelin that activates NPY neurons,

whereas it inhibits POMC and CART expression in the ARC (34, 57). Reduced ghrelin secretion may decrease *NPY* mRNA levels and increase *POMC* and *CART* mRNA levels in the ARC. These findings indicated that distinct underlying mechanisms may induce cachexia-associated anorexia development in different cachexia models.

In addition to body weight loss and anorexia, patients with cancer cachexia also exhibit a reduction in physical activity corresponding to daytime activities (22, 61). Similarly, locomotor activity in the "active period" or dark phase was substantially lower in 85As2-induced cachectic rats than in control rats, whereas locomotor activity was not different between these groups during the daytime period. Reduced activity during the dark phase, but not the light phase, in cachectic rats has also been observed in other cachexia models (41, 59). Because $\dot{V}_{O_2}$ is thought to be affected by the amount of locomotor activity, we evaluated this parameter during the daytime period. $\dot{V}_{O_2}$, RQ, and metabolic calorie levels were significantly higher in cachectic rats than in control rats during this time period. These findings suggested that enhanced energy expenditure, in addition to anorexia, may exacerbate body weight loss caused by the decrease in adipose and muscle tissues in cachectic rats. In fact, exacerbated resting energy expenditure in patients with cancer cachexia has frequently been observed (7, 8, 21) and is in contrast to the resting energy conservation associated with starvation-induced body weight loss.

Body weight maintenance is the most important end point of any treatment for cachexia-associated anorexia. Rikkunshito therapy has been shown to be an effective anorexia treatment in several animal models (50, 57); therefore, we evaluated the effect of rikkunshito on 85As2-induced cachexia symptoms. Rikkunshito substantially ameliorated cancer cachexia symptoms, including anorexia, weight loss, decreased water intake, and reductions in FFM, TBW, and musculature in the 85As2-induced cancer cachexia rat model; however, rikkunshito did not reduce tumor growth or plasma LIF levels. These findings indicated that the anticachectic effects of rikkunshito are not related to tumor regression or LIF levels. Rikkunshito has been shown to increase the secretion of ghrelin, an orexigenic hormone (57), and also to increase ghrelin receptor (GHSR) signaling efficacy (24). GHSR is expressed in the ARC and PVN of the hypothalamus, and ligand binding stimulates NPY/AgRP neurons, thereby transducing orexigenic signals to increase food intake. Thus, rikkunshito may ameliorate anorexia by activating GHSR-NPY/AgRP orexigenic signaling in the ARC and PVN. In fact, our previous study demonstrated that rikkunshito ameliorated cisplatin-induced anorexia in rats and reversed the cisplatin-induced decrease in hypothalamic orexigenic peptide mRNA levels (*NPY* in ARC) and increase in anorexigenic peptide mRNA levels (*POMC* and *CART* in the ARC) (65). Because anorexia induced by cancer cachexia and cisplatin may involve different mechanisms, further study is required to clarify the mechanisms by which rikkunshito ameliorates cancer cachexia-induced anorexia.

In conclusion, we established novel stomach cancer cachexia rat models by implanting nude rats with MKN45cl85 and 85As2 cells, both of which were derived from the human stomach cancer cell line MKN-45. The 85As2-induced cancer cachexia model, which was generated using peritoneal dissemination-derived 85As2 cells, induced earlier and more severe cachexia than the MKN45cl85 model, which may have been caused by differences in LIF production. The 85As2 model allowed for the early evaluation of cancer cachexia parameters associated with poor patient QOL and metabolic disturbances, such as anorexia and body weight loss (including low FFM). Our findings also indicate that rikkunshito may improve QOL in patients with stomach cancer cachexia. The 85As2 model should provide a useful tool for further study of cancer cachexia pathogenesis and treatment.

DISCLOSURES

Y. Uezono received grant support from Tsumura & Co. K. Terawaki and Y. Kase are employed by Tsumura & Co. Y. Sawada, Y. Kase, H. Hashimoto, M. Yoshimura, M. Suzuki, K. Miyano, Y. Sudo, S. Shiraishi, Y. Higami, K. Yanagihara, and Y. Ueta have no conflicts of interest to disclose.

AUTHOR CONTRIBUTIONS

K.T., Y. Sawada, Y. Kashiwase, H.H., M.Y., M.S., K.M., Y. Sudo, Y. Ueta, and Y. Uezono contributed to the conception and design of the research; K.T., Y. Sawada, Y. Kashiwase, H.H., M.Y., M.S., K.M., and Y. Sudo performed the experiments; K.T., Y. Sawada, Y. Kashiwase, H.H., M.Y., M.S., K.M., and Y. Sudo analyzed the data; K.T., Y. Sawada, Y. Kashiwase, H.H., M.Y., M.S., K.M., Y. Sudo, K.Y., and Y. Uezono interpreted the results of the experiments; K.T., Y. Sawada, Y. Kashiwase, H.H., and M.Y. prepared the figures; K.T. drafted the manuscript; K.T., S.S., Y.H., K.Y., Y. Ueta, and Y. Uezono edited and revised the manuscript; K.T., S.S., Y.H., K.Y., Y. Kase, Y. Ueta, and Y. Uezono approved the final version of manuscript.

REFERENCES

1. **Argilés JM, Olivan M, Busquets S, López-Soriano FJ.** Optimal management of cancer anorexia-cachexia syndrome. *Cancer Manag Res* 2: 27–38, 2010.
2. **Asp ML, Tian M, Wendel AA, Belury MA.** Evidence for the contribution of insulin resistance to the development of cachexia in tumor-bearing mice. *Int J Cancer* 126: 756–763, 2010.
3. **Auernhammer CJ, Melmed S.** Leukemia-inhibitory factor-neuroimmune modulator of endocrine function. *Endocr Rev* 21: 313–345, 2000.
4. **Bennani-Baiti N, Walsh D.** Animal models of the cancer anorexia-cachexia syndrome. *Support Care Cancer* 19: 1451–1463, 2011.
5. **Bo S, Dianliang Z, Hongmei Z, Xinxiang W, Yanbing Z, Xiaobo L.** Association of interleukin-8· gene polymorphism with cachexia from patients with gastric cancer. *J Interferon Cytokine Res* 30: 9–14, 2010.
6. **Bodine SC, Latres E, Baumhueter S, Lai VK, Nunez L, Clarke BA, Poueymirou WT, Panaro FJ, Na E, Dharmarajan K, Pan ZQ, Valenzuela DM, DeChiara TM, Stitt TN, Yancopoulos GD, Glass DJ.** Identification of ubiquitin ligases required for skeletal muscle atrophy. *Science* 294: 1704–1708, 2001.
7. **Bosaeus I, Daneryd P, Svanberg E, Lundholm K.** Dietary intake and resting energy expenditure in relation to weight loss in unselected cancer patients. *Int J Cancer* 93: 380–383, 2001.
8. **Cao DX, Wu GH, Zhang B, Quan YJ, Wei J, Jin H, Jiang Y, Yang ZA.** Resting energy expenditure and body composition in patients with newly detected cancer. *Clin Nutr* 29: 72–77, 2010.
9. **Chance WT, Balasubramaniam A, Borchers M, Fischer JE.** Refractory hypothalamic adenylate cyclase in anorectic tumor-bearing rats: implications for NPY-induced feeding. *Brain Res* 691: 180–184, 1995.

10. **Chance WT, Balasubramaniam A, Dayal R, Brown J, Fischer JE.** Hypothalamic concentration and release of neuropeptide Y into microdialysates is reduced in anorectic tumor-bearing rats. *Life Sci* 54: 1869–1874, 1994.

11. **Chance WT, Balasubramaniam A, Thompson H, Mohapatra B, Ramo J, Fischer JE.** Assessment of feeding response of tumor-bearing rats to hypothalamic injection and infusion of neuropeptide Y. *Peptides* 17: 797–801, 1996.

12. **Chance WT, Sheriff S, Kasckow JW, Regmi A, Balasubramaniam A.** NPY messenger RNA is increased in medial hypothalamus of anorectic tumor-bearing rats. *Regul Pept* 75–76: 347–353, 1998.

13. **Chang JW, Yeh KY, Shen YC, Hsieh JJ, Chuang CK, Liao SK, Tsai LH, Wang CH.** Production of multiple cytokines and induction of cachexia in athymic nude mice by a new anaplastic thyroid carcinoma cell line. *J Endocrinol* 179: 387–394, 2003.

14. **Chen SZ, Qiu ZG.** Combined treatment with GH, insulin, and indomethacin alleviates cancer cachexia in a mouse model. *J Endocrinol* 208: 131–136, 2011.

15. **Collins TJ.** ImageJ for microscopy. *BioTechniques* 43, 1 Suppl: 25–30, 2007.

16. **Costelli P, Muscaritoli M, Bossola M, Penna F, Reffo P, Bonetto A, Busquets S, Bonelli G, Lopez-Soriano FJ, Doglietto GB, Argilés JM, Baccino FM, Rossi Fanelli F.** IGF-1 is downregulated in experimental cancer cachexia. *Am J Physiol Regul Integr Comp Physiol* 291: R674–R683, 2006.

17. **Donohue E, Thomas A, Maurer N, Manisali I, Zeisser-Labouebe M, Zisman N, Anderson HJ, Ng SS, Webb M, Bally M, Roberge M.** The autophagy inhibitor verteporfin moderately enhances the antitumor activity of gemcitabine in a pancreatic ductal adenocarcinoma model. *J Cancer* 4: 585–596, 2013.

18. **dupont NC, Wang K, Wadhwa PD, Culhane JF, Nelson EL.** Validation and comparison of luminex multiplex cytokine analysis kits with ELISA: determinations of a panel of nine cytokines in clinical sample culture supernatants. *J Reprod Immunol* 66: 175–191, 2005.

19. **Ebrahimi B, Tucker SL, Li D, Abbruzzese JL, Kurzrock R.** Cytokines in pancreatic carcinoma: correlation with phenotypic characteristics and prognosis. *Cancer* 101: 2727–2736, 2004.

20. **Evans WJ, Morley JE, Argilés J, Bales C, Baracos V, Guttridge D, Jatoi A, Kalantar-Zadeh K, Lochs H, Mantovani G, Marks D, Mitch WE, Muscaritoli M, Najand A, Ponikowski P, Rossi Fanelli F, Schambelan M, Schols A, Schuster M, Thomas D, Wolfe R, Anker SD.** Cachexia: a new definition. *Clin Nutr* 27: 793–799, 2008.

21. **Falconer JS, Fearon KC, Plester CE, Ross JA, Carter DC.** Cytokines, the acute-phase response, and resting energy expenditure in cachectic patients with pancreatic cancer. *Ann Surg* 219: 325–331, 1994.

22. **Fouladiun M, Körner U, Gunnebo L, Sixt-Ammilon P, Bosaeus I, Lundholm K.** Daily physical-rest activities in relation to nutritional state, metabolism, and quality of life in cancer patients with progressive cachexia. *Clin Cancer Res* 13: 6379–6385, 2007.

23. **Fujitsuka N, Asakawa A, Hayashi M, Sameshima M, Amitani H, Kojima S, Fujimiya M, Inui A.** Selective serotonin reuptake inhibitors modify physiological gastrointestinal motor activities via 5-HT2c receptor and acyl ghrelin. *Biol Psychiatry* 65: 748–759, 2009.

24. **Fujitsuka N, Asakawa A, Uezono Y, Minami K, Yamaguchi T, Niijima A, Yada T, Maejima Y, Sedbazar U, Sakai T, Hattori T, Kase Y, Inui A.** Potentiation of ghrelin signaling attenuates cancer anorexia-cachexia and prolongs survival. *Transl Psychiatry* 1: e23, 2011.

25. **Gomes MD, Lecker SH, Jagoe RT, Navon A, Goldberg AL.** Atrogin-1, a muscle-specific F-box protein highly expressed during muscle atrophy. *Proc Natl Acad Sci USA* 98: 14440–14445, 2001.

26. **Graziano F, Ruzzo A, Santini D, Humar B, Tonini G, Catalano V, Berardi R, Pizzagalli F, Arduini F, Bearzi I, Scartozzi M, Cascinu S, Testa E, Ficarelli R, Magnani M.** Prognostic role of interleukin-1beta gene and interleukin-1 receptor antagonist gene polymorphisms in patients with advanced gastric cancer. *J Clin Oncol* 23: 2339–2345, 2005.

27. **Grossberg AJ, Scarlett JM, Zhu X, Bowe DD, Batra AK, Braun TP, Marks DL.** Arcuate nucleus proopiomelanocortin neurons mediate the acute anorectic actions of leukemia inhibitory factor via gp130. *Endocrinology* 151: 606–616, 2010.

28. **Hanada R, Teranishi H, Pearson JT, Kurokawa M, Hosoda H, Fukushima N, Fukue Y, Serino R, Fujihara H, Ueta Y, Ikawa M, Okabe M, Murakami N, Shirai M, Yoshimatsu H, Kangawa K, Kojima M.** Neuromedin U has a novel anorexigenic effect independent of the leptin signaling pathway. *Nat Med* 10: 1067–1073, 2004.

29. **Harasawa S, Miyoshi A, Miwa T, et al.** Double-blind multicenter post-marketing clinical trial of TJ-43 TSUMURA Rikkunshi-to for the treatment of dysmotility-like dyspepsia. *J Clin Exp Med* 187: 207–229, 1998.

30. **Harbuz MS, Chalmers J, De Souza L, Lightman SL.** Stress-induced activation of CRF and c-fos mRNAs in the paraventricular nucleus are not affected by serotonin depletion. *Brain Res* 609: 167–173, 1993.

31. **Hashimoto H, Azuma Y, Kawasaki M, Fujihara H, Onuma E, Yamada-Okabe H, Takuwa Y, Ogata E, Ueta Y.** Parathyroid hormone-related protein induces cachectic syndromes without directly modulating the expression of hypothalamic feeding-regulating peptides. *Clin Cancer Res* 13: 292–298, 2007.

32. **Hayakawa T, Arakawa T, Kase Y, Akiyama S, Ishige A, Takeda S, Sasaki H, Uno H, Fukuda T, Higuchi K, Kobayashi K.** Liu-Jun-Zi-Tang, a kampo medicine, promotes adaptive relaxation in isolated guinea pig stomachs. *Drugs Exp Clin Res* 25: 211–218, 1999.

33. **Inokuma K, Okamatsu-Ogura Y, Omachi A, Matsushita Y, Kimura K, Yamashita H, Saito M.** Indispensable role of mitochondrial UCP1 for antiobesity effect of β3-adrenergic stimulation. *Am J Physiol Endocrinol Metab* 290: E1014–E1021, 2006.

34. **Kojima M, Kangawa K.** Ghrelin: structure and function. *Physiol Rev* 85: 495–522, 2005.

35. **Laviano A, Meguid MM, Inui A, Muscaritoli M, Rossi-Fanelli F.** Therapy insight: Cancer anorexia-cachexia syndrome—when all you can eat is yourself. *Nat Clin Pract Oncol* 2: 158–165, 2005.

36. **Liu CM, Yang Z, Liu CW, Wang R, Tien P, Dale R, Sun LQ.** Effect of RNA oligonucleotide targeting Foxo-1 on muscle growth in normal and cancer cachexia mice. *Cancer Gene Ther* 14: 945–952, 2007.

37. **Livak KJ, Schmittgen TD.** Analysis of relative gene expression data using real-time quantitative PCR and the 2(−Delta Delta C(T)) Method. *Methods* 25: 402–408, 2001.

38. **McCarthy HD, McKibbin PE, Perkins AV, Linton EA, Williams G.** Alterations in hypothalamic NPY and CRF in anorexic tumor-bearing rats. *Am J Physiol Endocrinol Metab* 264: E638–E643, 1993.

39. **Mori M, Yamaguchi K, Abe K.** Purification of a lipoprotein lipase-inhibiting protein produced by a melanoma cell line associated with cancer cachexia. *Biochem Biophys Res Commun* 160: 1085–1092, 1989.

40. **Mori M, Yamaguchi K, Honda S, Nagasaki K, Ueda M, Abe O, Abe K.** Cancer cachexia syndrome developed in nude mice bearing melanoma cells producing leukemia-inhibitory factor. *Cancer Res* 51: 6656–6659, 1991.

41. **Murphy KT, Chee A, Trieu J, Naim T, Lynch GS.** Importance of functional and metabolic impairments in the characterization of the C-26 murine model of cancer cachexia. *Dis Model Mech* 5: 533–545, 2012.

42. **Muscaritoli M, Bossola M, Aversa Z, Bellantone R, Rossi Fanelli F.** Prevention and treatment of cancer cachexia: new insights into an old problem. *Eur J Cancer* 42: 31–41, 2006.

43. **Nomura M, Ueta Y, Serino R, Kabashima N, Shibuya I, Yamashita H.** PACAP type I receptor gene expression in the paraventricular and supraoptic nuclei of rats. *Neuroreport* 8: 67–70, 1996.

44. **Ohno T, Yanai M, Ando H, Toyomasu Y, Ogawa A, Morita H, Ogata K, Mochiki E, Asao T, Kuwano H.** Rikkunshito, a traditional Japanese medicine, suppresses cisplatin-induced anorexia in humans. *Clin Exp Gastroenterol* 4: 291–296, 2011.

45. **Oike Y, Akao M, Yasunaga K, Yamauchi T, Morisada T, Ito Y, Urano T, Kimura Y, Kubota Y, Maekawa H, Miyamoto Y, Miyata K, Matsumoto S, Sakai J, Nakagata N, Takeya M, Koseki H, Ogawa Y, Kadowaki T, Suda T.** Angiopoietin-related growth factor antagonizes obesity and insulin resistance. *Nat Med* 11: 400–408, 2005.

46. **Okada S, Okusaka T, Ishii H, Kyogoku A, Yoshimori M, Kajimura N, Yamaguchi K, Kakizoe T.** Elevated serum interleukin-6 levels in patients with pancreatic cancer. *Jpn J Clin Oncol* 28: 12–15, 1998.

47. **Pan W, Kastin AJ, Brennan JM.** Saturable entry of leukemia inhibitory factor from blood to the central nervous system. *J Neuroimmunol* 106: 172–180, 2000.

48. **Paxinos G, Watson C.** *The Rat Brain in Stereotaxic Coordinatesed.* Sydney, Australia: Academic, 1982.

49. **Reed SA, Sandesara PB, Senf SM, Judge AR.** Inhibition of FoxO transcriptional activity prevents muscle fiber atrophy during cachexia and induces hypertrophy. *FASEB J* 26: 987–1000, 2012.

50. **Scarlett JM, Zhu X, Enriori PJ, Bowe DD, Batra AK, Levasseur PR, Grant WF, Meguid MM, Cowley MA, Marks DL.** Regulation of agouti-related protein messenger ribonucleic acid transcription and peptide

secretion by acute and chronic inflammation. *Endocrinology* 149: 4837–4845, 2008.

51. **Scott HR, McMillan DC, Crilly A, McArdle CS, Milroy R.** The *relationship between weight loss and interleukin 6 in non-small-cell lung cancer. Br J Cancer* 73: 1560–1562, 1996.

52. **Smith DL Jr, Johnson MS, Nagy TR.** Precision and accuracy of bioimpedance spectroscopy for determination of in vivo body composition in rats. *Int J Body Compos Res* 7: 21–26, 2009.

53. **Soda K, Kawakami M, Kashii A, Miyata M.** Manifestations of cancer cachexia induced by colon 26 adenocarcinoma are not fully ascribable to interleukin-6. *Int J Cancer* 62: 332–336, 1995.

54. **Sun F, Sun Y, Yu Z, Zhang D, Zhang J, Song B, Zheng H.** Interleukin-10 gene polymorphisms influence susceptibility to cachexia in patients with low-third gastric cancer in a Chinese population. *Mol Diagn Ther* 14: 95–100, 2010.

55. **Suzuki H, Hashimoto H, Kawasaki M, Watanabe M, Otsubo H, Ishikura T, Fujihara H, Ohnishi H, Onuma E, Yamada-Okabe H, Takuwa Y, Ogata E, Nakamura T, Ueta Y.** Similar changes of hypothalamic feeding-regulating peptides mRNAs and plasma leptin levels in PTHrP-, LIF-secreting tumors-induced cachectic rats and adjuvant arthritic rats. *Int J Cancer* 128: 2215–2223, 2011.

56. **Suzuki M, Narita M, Ashikawa M, Furuta S, Matoba M, Sasaki H, Yanagihara K, Terawaki K, Suzuki T, Uezono Y.** Changes in the melanocortin receptors in the hypothalamus of a rat model of cancer cachexia. *Synapse* 66: 747–751, 2012.

57. **Takeda H, Sadakane C, Hattori T, Katsurada T, Ohkawara T, Nagai K, Asaka M.** Rikkunshito, an herbal medicine, suppresses cisplatin-induced anorexia in rats via 5-HT2 receptor antagonism. *Gastroenterology* 134: 2004–2013, 2008.

58. **Tisdale MJ.** Mechanisms of cancer cachexia. *Physiol Rev* 89: 381–410, 2009.

59. **Toledo M, Busquets S, Sirisi S, Serpe R, Orpí M, Coutinho J, Martínez R, López-Soriano FJ, Argilés JM.** Cancer cachexia: physical activity and muscle force in tumour-bearing rats. *Oncol Rep* 25: 189–193, 2011.

60. **Tominaga K, Kido T, Ochi M, Sadakane C, Mase A, Okazaki H, Yamagami H, Tanigawa T, Watanabe K, Watanabe T, Fujiwara Y, Oshitani N, Arakawa T.** The Traditional Japanese Medicine Rikkunshito Promotes Gastric Emptying via the Antagonistic Action of the 5-HT(3) Receptor Pathway in Rats. *Evid Based Complement Alternat Med* 2011: 248481, 2011.

61. **van Norren K, Kegler D, Argiles JM, Luiking Y, Gorselink M, Laviano A, Arts K, Faber J, Jansen H, van der Beek EM, van Helvoort A.** Dietary supplementation with a specific combination of high protein, leucine, and fish oil improves muscle function and daily activity in tumour-bearing cachectic mice. *Br J Cancer* 100: 713–722, 2009.

62. **Yamamoto Y, Ueta Y, Yamashita H, Asayama K, Shirahata A.** Expressions of the prepro-orexin and orexin type 2 receptor genes in obese rat. *Peptides* 23: 1689–1696, 2002.

63. **Yanagihara K, Takigahira M, Mihara K, Kubo T, Morimoto C, Morita Y, Terawaki K, Uezono Y, Seyama T.** Inhibitory effects of isoflavones on tumor growth and cachexia in newly established cachectic mouse models carrying human stomach cancers. *Nutr Cancer* 65: 578–589, 2013.

64. **Yanai M, Mochiki E, Ogawa A, Morita H, Toyomasu Y, Ogata K, Tabe Y, Ando H, Ohno T, Asao T, Aomori T, Fujita Y, Kuwano H.** Intragastric administration of rikkunshito stimulates upper gastrointestinal motility and gastric emptying in conscious dogs. *J Gastroenterol* 48: 611–619, 2013.

65. **Yoshimura M, Matsuura T, Ohkubo J, Ohno M, Maruyama T, Ishikura T, Hashimoto H, Kakuma T, Yoshimatsu H, Terawaki K, Uezono Y, Ueta Y.** The gene expression of the hypothalamic feeding-regulating peptides in cisplatin-induced anorexic rats. *Peptides* 46: 13–19, 2013.

66. **Zaki MH, Nemeth JA, Trikha M.** CNTO 328, a monoclonal antibody to IL-6, inhibits human tumor-induced cachexia in nude mice. *Int J Cancer* 111: 592–595, 2004.

The Endocannabinoid Anandamide Inhibits Voltage-Gated Sodium Channels Na$_v$1.2, Na$_v$1.6, Na$_v$1.7, and Na$_v$1.8 in *Xenopus* Oocytes

Dan Okura, MD,* Takafumi Horishita, MD, PhD,* Susumu Ueno, MD, PhD,† Nobuyuki Yanagihara, PhD,‡ Yuka Sudo, PhD,§ Yasuhito Uezono, MD, PhD,‖ and Takeyoshi Sata, MD, PhD*

BACKGROUND: Anandamide is an endocannabinoid that regulates multiple physiological functions by pharmacological actions, in a manner similar to marijuana. Recently, much attention has been paid to the analgesic effect of endocannabinoids in terms of identifying new pharmacotherapies for refractory pain management, but the mechanisms of the analgesic effects of anandamide are still obscure. Voltage-gated sodium channels are believed to play important roles in inflammatory and neuropathic pain. We investigated the effects of anandamide on 4 neuronal sodium channel α subunits, Na$_v$1.2, Na$_v$1.6, Na$_v$1.7, and Na$_v$1.8, to explore the mechanisms underlying the antinociceptive effects of anandamide.

METHODS: We studied the effects of anandamide on Na$_v$1.2, Na$_v$1.6, Na$_v$1.7, and Na$_v$1.8 α subunits with β$_1$ subunits by using whole-cell, 2-electrode, voltage-clamp techniques in *Xenopus* oocytes.

RESULTS: Anandamide inhibited sodium currents of all subunits at a holding potential causing half-maximal current (V$_{1/2}$) in a concentration-dependent manner. The half-maximal inhibitory concentration values for Na$_v$1.2, Na$_v$1.6, Na$_v$1.7, and Na$_v$1.8 were 17, 12, 27, and 40 μmol/L, respectively, indicating an inhibitory effect on Na$_v$1.6, which showed the highest potency. Anandamide raised the depolarizing shift of the activation curve as well as the hyperpolarizing shift of the inactivation curve in all α subunits, suggesting that sodium current inhibition was due to decreased activation and increased inactivation. Moreover, anandamide showed a use-dependent block in Na$_v$1.2, Na$_v$1.6, and Na$_v$1.7 but not Na$_v$1.8.

CONCLUSION: Anandamide inhibited the function of α subunits in neuronal sodium channels Na$_v$1.2, Na$_v$1.6, Na$_v$1.7, and Na$_v$1.8. These results help clarify the mechanisms of the analgesic effects of anandamide. (Anesth Analg 2014;118:554–62)

C annabis has been used as a pleasure-inducing drug and traditional medicine for thousands of years, and since the 2 cannabinoid receptors CB$_1$[1,2] and CB$_2$[3] were identified, the endocannabinoid signaling system has been a focus of medical research and has been considered a potential therapeutic target.[4] Endocannabinoids mimic the pharmacological actions of the psychoactive principle agent in marijuana, Δ^9-tetrahydrocannabinol, and regulate multiple physiological functions, such as analgesia, regulation of food intake, immunomodulation, inflammation, addictive behavior, epilepsy, and others.[5]

Anandamide, the ethanolamide of arachidonic acid, was the first endocannabinoid isolated from the brain[6]; it acts as a partial agonist on CB$_1$ receptors, with a lesser effect on CB$_2$ receptors.[7] Several groups have shown an analgesic effect of exogenous anandamide through the CB$_1$ receptor in acute,[8–10] persistent inflammatory,[11–13] and neuropathic pain models.[14,15] CB$_1$ receptors are distributed throughout the pain pathways of the central nervous system (CNS), including the periaqueductal gray, amygdala, and spinal trigeminal tract,[16,17] and the peripheral nervous system including the dorsal root ganglion (DRG),[18] suggesting an analgesic effect of anandamide via CB$_1$ receptors. However, anandamide may also act on other ion channels consisting of pain signaling pathways, including voltage-gated Ca^{2+} channels, TASK1 channels, 5-HT$_3$ receptor, rectifying K$^+$ channels, and N-methyl-D-aspartate receptors[19–24]; thus, the mechanisms of the analgesic effects of anandamide remain unclear.

Voltage-gated sodium channels play an essential role in action potential initiation and propagation in excitable nerve and muscle cells. Nine distinct pore-forming α subunits (Na$_v$1.1–Na$_v$1.9), which are associated with auxiliary β subunits, have been identified,[25,26] and each has a different pattern of development and localization as well as distinct physiological and pathophysiological roles. Sodium channel α subunits expressed in DRG (Na$_v$1.7, Na$_v$1.8, Na$_v$1.9) are believed to play crucial roles in inflammatory and neuropathic pain and are considered potential targets of these conditions.[27–30] Previous studies have shown that anandamide inhibits sodium channel function in the brain through the inhibition of veratridine-dependent depolarization of synaptosomes[31] and suppresses tetrodotoxin-sensitive (TTX-S) and tetrodotoxin-resistant (TTX-R) sodium currents in rat

DRG neurons.[32] These results suggest that sodium channels are potential targets for anandamide. However, the precise mechanisms of anandamide on each α subunit are still unknown. It is of great importance to clarify these mechanisms because each α subunit has a difference of 20% to 50% in amino acid sequence in the transmembrane and extracellular domains and therefore has different physiological functions. Here, we explored the effects of anandamide on several sodium channel α subunits, including $Na_v1.2$, that is expressed primarily in the CNS; $Na_v1.6$ that is expressed in the CNS and DRG neurons; and $Na_v1.7$ and $Na_v1.8$ that are expressed in DRG neurons.

METHODS

This study was approved by the Animal Research Committee of the University of Occupational and Environmental Health.

Materials

Adult female *Xenopus laevis* frogs were obtained from Kyudo Co., Ltd. (Saga, Japan). Anandamide was purchased from Sigma-Aldrich (St. Louis, MO). Rat $Na_v1.2$ α subunit cDNA was a gift from Dr. W. A. Catterall (University of Washington, Seattle, WA). Rat $Na_v1.6$ α subunit cDNA was a gift from Dr. A. L. Goldin (University of California, Irvine, CA). Rat $Na_v1.7$ α subunit cDNA was a gift from G. Mandel (Oregon Health and Science University, Portland, OR). Rat $Na_v1.8$ α subunit cDNA was a gift from Dr. A. N. Akopian (University of Texas Health Science Center, San Antonio, TX), and human $β_1$ subunit cDNA was a gift from Dr. A. L. George (Vanderbilt University, Nashville, TN).

cRNA Preparation and Oocyte Injection

After linearization of cDNA with *Cla*I ($Na_v1.2$ α subunit), *Not*I ($Na_v1.6$, 1.7 α subunit), *Xba*I ($Na_v1.8$ α subunit), and *Eco*RI ($β_1$ subunit), cRNAs were transcribed by using SP6 (1.8 α, $β_1$ subunit) or T7 ($Na_v1.2$, 1.6 1.7 α subunit) RNA polymerase from the mMESSAGE mMACHINE kit (Ambion, Austin, TX). Preparation of *X. laevis* oocytes and cRNA microinjection were performed as described previously.[33] Briefly, stage IV to VI oocytes were manually isolated from a removed portion of ovary. Next, oocytes were treated with collagenase (0.5 mg/mL) for 10 minutes and placed in modified Barth's solution (88 mmol/L NaCl, 1 mmol/L KCl, 2.4 mmol/L $NaHCO_3$, 10 mmol/L HEPES, 0.82 mmol/L $MgSO_4$, 0.33 mmol/L $Ca(NO_3)_2$, and 0.91 mmol/L $CaCl_2$, adjusted to pH 7.5), supplemented with 10,000 U penicillin, 50 mg gentamicin, 90 mg theophylline, and 220 mg sodium pyruvate per liter (incubation medium). Na_v α subunit cRNAs were coinjected with $β_1$ subunit cRNA at a ratio of 1:10 (total volume was 20–40 ng/50 nL) into *Xenopus* oocytes (all α subunits were coinjected with the $β_1$ subunit). Injected oocytes were incubated at 19°C in incubation medium, and 2 to 6 days after injection, the cells were used for electrophysiological recordings.

Electrophysiological Recordings

All electrical recordings were performed at room temperature (23°C). Oocytes were placed in a 100 μL recording chamber and perfused at 2 mL/min with Frog Ringer's solution containing 115 mmol/L NaCl, 2.5 mmol/L KCl, 10 mmol/L HEPES, 1.8 mmol/L $CaCl_2$, pH 7.2, by using a peristaltic pump (World Precision Instruments Inc., Sarasota, FL). Recording electrodes were prepared with borosilicate glass by using a puller (PP-830, Narishige group company, Tokyo, Japan), and microelectrodes were filled with 3 mol KCl/0.5% low-melting-point agarose with resistances between 0.3 and 0.5 MΩ. The whole-cell voltage clamp was achieved through these 2 electrodes by using a Warner Instruments model OC-725C (Warner, Hamden, CT). Currents were recorded and analyzed by using pCLAMP 7.0 software (Axon Instruments, Foster City, CA), and the amplitude of expressed sodium currents was typically 2 to 15 μA. Transients and leak currents were subtracted by using the P/N procedure. Anandamide stocks were prepared in dimethylsulphoxide (DMSO) and diluted in Frog Ringer's solution to a final DMSO concentration not exceeding 0.05%. Anandamide was then perfused for 5 to 10 minutes to reach equilibrium.

The voltage dependence of activation was determined by using 50-millisecond depolarizing pulses from a holding potential causing maximal current, V_{max} (–90 mV for $Na_v1.2$ and $Na_v1.6$ or –100 mV for $Na_v1.7$ and $Na_v1.8$), and from a holding potential causing half-maximal current, $V_{1/2}$ (from approximately –40 mV to –70 mV) to 50 mV in 10 mV increments. Normalized activation curves were fitted to the Boltzmann equation: $G/G_{max} = 1/(1 + exp(V_{1/2} – V)/k)$, where G is the voltage-dependent sodium conductance, G_{max} is the maximal sodium conductance, G/G_{max} is the normalized fractional conductance, $V_{1/2}$ is the potential at which activation is half maximal, and k is the slope factor. The G value for each oocyte was calculated by using the formula $G = I/(Vt – Vr)$, where I is the peak sodium current, Vt is the test potential and Vr is the reversal potential. The Vr for each oocyte was estimated by extrapolating the linear ascending segment of the current voltage relationship (I–V) curve to the voltage axis. To measure steady-state inactivation, currents were elicited by a 50-millisecond test pulse to –20 mV for $Na_v1.2$ and $Na_v1.6$ or –10 mV for $Na_v1.7$ or +10 mV for $Na_v1.8$ after 200 milliseconds (500 milliseconds for only $Na_v1.8$) prepulses ranging from –140 mV to 0 mV in 10 mV increments from a holding potential of V_{max}. Steady-state inactivation curves were fitted to the Boltzmann equation: $I/I_{max} = 1/(1 + exp(V_{1/2} – V)/k)$, where I_{max} is the maximal sodium current, I/I_{max} is the normalized current, $V_{1/2}$ is the voltage of half-maximal inactivation, and k is the slope factor. To investigate a use-dependent sodium channel block of anandamide, currents were elicited at 10 Hz by a 20-millisecond depolarizing pulse of –20 mV for $Na_v1.2$ and $Na_v1.6$ or –10 mV for $Na_v1.7$ or +10 mV for $Na_v1.8$ from a $V_{1/2}$ holding potential in both the absence and presence of 30 μmol/L anandamide. Peak currents were measured and normalized to the first pulse and plotted against the pulse number. Data were fitted to the monoexponential equation $I_{Na} = exp(–τ_{use}·n) + C$, where n is pulse number, C is the plateau I_{Na}, and $τ_{use}$ is the time constant of use-dependent decay.

Data Analysis

All values are presented as the mean ± SEM ($n = 5$–8). The n values refer to the number of oocytes examined. Each experiment was performed with oocytes from at least 2 frogs.

Control sodium current recorded in absence of anandamide was assigned a value of 100%. Data were statistically evaluated by paired t test by using GraphPad Prism software (GraphPad Software, Inc., San Diego, CA). Hill slope and half-maximal inhibitory concentration values were also calculated by using this software.

RESULTS

Effects of Anandamide on Peak Na+ Inward Currents

Currents were elicited by using a 50-millisecond depolarizing pulse to −20 mV for $Na_v1.2$ and $Na_v1.6$ or −10 mV for $Na_v1.7$ or +10 mV for $Na_v1.8$ applied every 10 seconds from V_{max} or $V_{1/2}$ holding potential in both the absence and presence of 10 µmol/L anandamide (Fig. 1); anandamide was applied for 10 minutes. Anandamide inhibited the peak I_{Na} induced by all α subunits more potently at $V_{1/2}$ than V_{max}. Anandamide reduced the peak I_{Na} induced by $Na_v1.2$, $Na_v1.6$, $Na_v1.7$, and $Na_v1.8$ by 46 ± 4, 49 ± 3, 37 ± 2, and 27 ± 2 at $V_{1/2}$, respectively, and 7 ± 2, 6 ± 1, 9 ± 1, and 21 ± 5% at V_{max}, respectively (Fig. 2). Inhibition of anandamide at $V_{1/2}$ was statistically significant in all α subunits, but those at V_{max} were not statistically significant except for the suppression in $Na_v1.8$ by paired t test. Because suppression at $V_{1/2}$ was potent, we examined the concentration-response relation for anandamide inhibition of the peak I_{Na} induced by $Na_v1.2$, $Na_v1.6$, $Na_v1.7$, and $Na_v1.8$ at $V_{1/2}$ holding potential (Fig. 3). The peak current amplitude in the presence of anandamide was normalized to that in the control, and the effects of anandamide were expressed as percentages of the control. Nonlinear regression analyses of the dose-response curves yielded half-maximal inhibitory concentration values and Hill slopes of 17 ± 3 µmol/L and 0.74 ± 0.04 for $Na_v1.2$, 12 ± 1 µmol/L and 0.79 ± 0.08 for $Na_v1.6$, 27 ± 3 µmol/L and 0.52 ± 0.06 for $Na_v1.7$, 40 ± 14 µmol/L and 0.71 ± 0.10 for $Na_v1.8$, respectively (Fig. 3).

Effects of Anandamide on Sodium Current Activation

We examined the effects of anandamide on 4 α subunits of sodium current activation. Voltage dependence of activation was determined by using 50-millisecond depolarizing pulses from a holding potential of V_{max} to 50 mV in 10 mV increments or from a holding potential of $V_{1/2}$ to 50 mV in 10 mV increments for $Na_v1.2$, $Na_v1.6$, $Na_v1.7$, and $Na_v1.8$. Activation curves were derived from the I-V curves (see Methods); anandamide (30 µmol/L) was applied for 5 minutes. The peak I_{Na} was reduced by anandamide at V_{max} and $V_{1/2}$ holding potentials with all subunits (Fig. 4). Anandamide shifted the midpoint of steady-state activation ($V_{1/2}$) in a depolarizing direction at both holding potentials for all subunits (Fig. 5). These shifts were small (1.9–3.8 mV) but statistically significant (Table 1).
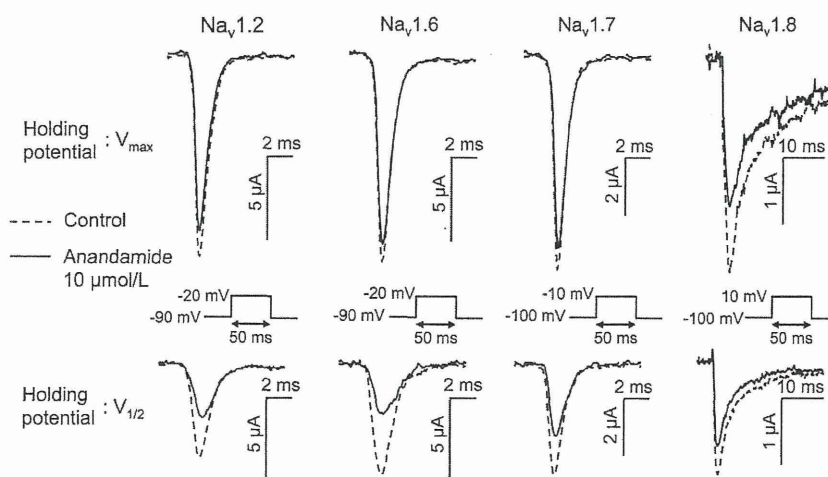
Effects of Anandamide on Sodium Current Inactivation

The effect of anandamide on steady-state inactivation was also investigated. Currents were elicited by a 50-millisecond test pulse to −20 mV for $Na_v1.2$ and $Na_v1.6$ or −10 mV for $Na_v1.7$ or +10 mV for $Na_v1.8$ after 200 millis econds(500 milliseconds for only $Na_v1.8$) prepulses ranging from −140 mV to 0 mV in 10 mV increments from a holding potential of V_{max}. Steady-state inactivation curves were fitted to the Boltzmann equation (see Methods); anandamide (30 µmol/L) was applied for 5 minutes. Anandamide significantly shifted the midpoint of steady-state inactivation ($V_{1/2}$) in the hyperpolarizing direction by 5.2, 5.0, 4.1, and 6.3 mV in $Na_v1.2$, $Na_v1.6$, $Na_v1.7$, and $Na_v1.8$, respectively (Fig. 6, Table 1).

Use-Dependent Block of Sodium Currents by Anandamide

We investigated the use-dependent block of sodium currents by anandamide. Currents were elicited at 10 Hz by a 20-millisecond depolarizing pulse of −20 mV for $Na_v1.2$ and $Na_v1.6$ or −10 mV for $Na_v1.7$ or +10 mV for $Na_v1.8$ from a $V_{1/2}$ holding potential in both the absence and presence of 30 µmol/L anandamide. Peak currents were measured and normalized to the first pulse and plotted against the pulse number (Fig. 7, A–D). Data were fitted by the monoexponential equation (see Methods); anandamide was applied for 5 minutes. Anandamide significantly reduced the plateau I_{Na} amplitude of $Na_v1.2$, $Na_v1.6$, and $Na_v1.7$ from 0.74 ± 0.02 to 0.66 ± 0.03, 0.88 ± 0.01 to 0.66 ± 0.02, and 0.73 ±

Figure 1. Inhibitory effects of anandamide on peak sodium inward currents in *Xenopus* oocytes expressing $Na_v1.2$, $Na_v1.6$, $Na_v1.7$, and $Na_v1.8$ α subunits with $β_1$ subunits at 2 holding potentials. Representative traces are shown. Sodium currents were evoked by 50-millisecond depolarizing pulses to −20 mV for $Na_v1.2$ and $Na_v1.6$ or −10 mV for $Na_v1.7$ or +10 mV for $Na_v1.8$ from V_{max} holding potential (upper panel) or $V_{1/2}$ holding potential (lower panel) in both the absence and presence of 10 µmol/L anandamide; anandamide was applied for 10 minutes.
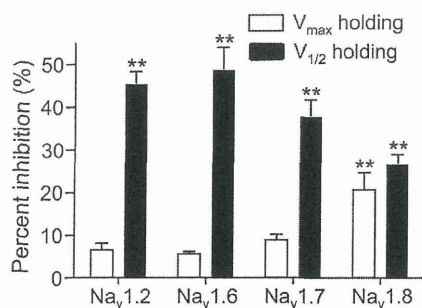
Figure 2. Inhibitory effects of anandamide on peak sodium inward currents in *Xenopus* oocytes expressing $Na_v1.2$, $Na_v1.6$, $Na_v1.7$, and $Na_v1.8$ α subunits with $β_1$ subunits at 2 holding potentials. Percent inhibition of sodium current of anandamide was calculated. Open columns represent the effect at V_{max} holding potential, and closed columns indicate the effect at $V_{1/2}$ holding potential. Anandamide inhibited the peak I_{Na} induced by $Na_v1.2$, $Na_v1.6$, $Na_v1.7$, and $Na_v1.8$ by 46 ± 4, 49 ± 3, 37 ± 2, and 27 ± 2 at $V_{1/2}$, respectively, and 7 ± 2, 6 ± 1, 9 ± 1, and 21 ± 5% at V_{max}, respectively. Data are represented as the mean ± SEM (n = 5–7). **P < 0.01, compared with the control (based on paired t test).
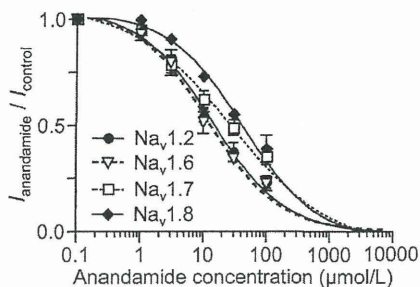

Figure 3. Concentration-response curves for anandamide suppression of sodium currents elicited by 50-millisecond depolarizing pulses to –20 mV for $Na_v1.2$ and $Na_v1.6$ or –10 mV for $Na_v1.7$ or +10 mV for $Na_v1.8$ from $V_{1/2}$ holding potential. The peak current amplitude in the presence of anandamide was normalized to that in the control, and the effects of anandamide are expressed as percentages of the control. Half-maximal inhibitory concentration values and Hill slopes were 17 ± 3 μmol/L and 0.74 ± 0.04 for $Na_v1.2$, 12 ± 1 μmol/L and 0.79 ± 0.08 for $Na_v1.6$, 27 ± 3 μmol/L and 0.52 ± 0.06 for $Na_v1.7$, and 40 ± 14 μmol/L and 0.71 ± 0.10 for $Na_v1.8$, respectively. Data are represented as the mean ± SEM (n = 5–8). Data were fit to the Hill slope equation to give the half-maximal inhibitory concentration values and Hill slopes. Half-maximal inhibitory concentration values and Hill slopes were calculated by using GraphPad Prism.

0.03 to 0.57 ± 0.04, respectively (Fig. 7E), demonstrating a use-dependent block, whereas anandamide did not reduce the plateau I_{Na} amplitude of $Na_v1.8$ (from 0.86 ± 0.03 to 0.84 ± 0.04).

DISCUSSION

In the present study, we demonstrated that anandamide suppresses the $Na_v1.2$, $Na_v1.6$, $Na_v1.7$, and $Na_v1.8$ α subunits in a concentration-dependent manner. half-maximal inhibitory concentration values ranged from 12 μmol/L ($Na_v1.6$) to 40 μmol/L ($Na_v1.8$). Wiley et al.[34] have reported that IV administration of anandamide produce a dose-dependent antinociceptive effect in the tail-flick test with mice, and the 50% effective dose (ED_{50}) of that was 15 mg/kg. They also have shown that the plasma concentration of anandamide was 4.96 μg/mL (14.3 μmol/L) when

10 mg/kg of anandamide was administered, suggesting that half-maximal inhibitory concentration values used in the present study are pharmacologically relevant and are close to the plasma concentration exhibiting an antinociceptive effect by anandamide. We also demonstrated that anandamide has more potent inhibitory effects on sodium currents at $V_{1/2}$ holding potential (inactivated state) than at V_{max} holding potential (resting state) in a manner similar to that of local anesthetics on sodium channels. Therefore, the analgesic effects of anandamide may be mediated through sodium channel blockade. The present results are partially consistent with previous reports that anandamide suppresses TTX-S veratridine-dependent depolarization of synaptosomes, the binding of batrachotoxin to sodium channels, and TTX-S sustained repetitive firing in cortical neurons[31] and inhibits TTX-S and TTX-R sodium currents in a concentration-dependent manner in rat DRG neurons.[32] However, their precise mechanisms of anandamide on several sodium channel α subunits have not yet been investigated. Considering that $Na_v1.6$ was distributed in both CNS and DRG neurons, and that $Na_v1.8$ was distributed in DRG neurons, our results are consistent with a previous study showing that anandamide inhibited sodium currents with half-maximal inhibitory concentration values of 5.4 μmol/L for the TTX-S current and 38 μmol/L for the TTX-R current in DRG neurons,[32] suggesting that TTX-S and TTX-R currents in DRG neurons may represent $Na_v1.6$ and $Na_v1.8$ currents, respectively. Because $Na_v1.6$ is expressed in both the brain and DRG, and anandamide suppressed $Na_v1.6$ function most potently among the 4 α subunits, the effect of anandamide on $Na_v1.6$ may be the most important.

The effects of anandamide on channel gating, including activation and inactivation, demonstrated common characteristics among the 4 α subunits we studied. Anandamide shifted the midpoint of steady-state activation ($V_{1/2}$) in a depolarizing direction at both $V_{1/2}$ and V_{max} holding potentials for all α subunits, and the shifts were significant, although the shifts were small (approximately 4 mV). Anandamide also significantly shifted the midpoint of steady-state inactivation ($V_{1/2}$) in the hyperpolarizing direction (approximately 7 mV) for all α subunits. These results suggest that both inhibition of activation and the enhancement of inactivation are common mechanisms of sodium current inhibition by anandamide for $Na_v1.2$, $Na_v1.6$, $Na_v1.7$, and $Na_v1.8$. A combination of effects on both activation and inactivation might produce sufficient effects to suppress sodium currents although each effect is small. Inhibition by anandamide at V_{max} holding potential for $Na_v1.2$, $Na_v1.6$, and $Na_v1.7$ was small and not significant, whereas that for $Na_v1.8$ was significant (Fig. 1), indicating that resting-channel block is one of the important mechanisms of anandamide inhibition for only $Na_v1.8$. Anandamide exhibited use-dependent block with repetitive stimuli for $Na_v1.2$, $Na_v1.6$, and $Na_v1.7$ but not $Na_v1.8$. The presence of use-dependent block by anandamide suggests the possibility of open-channel block and the ability to slow the recovery time from blocks that are seen with amitriptyline.[35] Sodium channel blockers such as local anesthetics, tricyclic antidepressants, and volatile anesthetics have been shown to shift the voltage dependence of steady-state inactivation with no effect on